Ceramics International 51 (2025) 20518–20531

Contents lists available at ScienceDirect

Ceramics International

journal homepage: www.elsevier.com/locate/ceramint

Room-temperature synthesis of refractory borides: A case study on mechanochemistry and characterization of Mo-borides and W-borides

İlayda Süzer [a,*,1], Amir Akbari [a,1], Faruk Kaya [b], Sıddıka Mertdinç-Ülküseven [a], Bora Derin [b], M. Lütfi Öveçoğlu [a,c], Duygu Ağaoğulları [a,**]

[a] Istanbul Technical University, Faculty of Chemical and Metallurgical Engineering, Department of Metallurgical and Materials Engineering, Particulate Materials Laboratories (PML), Graphene & 2D Materials Laboratory, Maslak, Istanbul, 34469, Türkiye
[b] Istanbul Technical University, Department of Metallurgical and Materials Engineering, Maslak, Istanbul, 34469, Türkiye
[c] MEF University, Department of Mechanical Engineering, Sarıyer, Istanbul, 34396, Türkiye

ARTICLE INFO

Handling Editor: Dr P. Vincenzini

Keywords:
Mechanochemical synthesis
Thermochemical calculation
Leaching
Refractory borides
Microstructure
X-ray methods

ABSTRACT

Mo-boride and W-boride powders were produced from native boron oxide, magnesium, and related metal oxide starting materials by mechanochemical synthesis (MCS) followed by an purification treatment. The reaction formation mechanisms and the products were predicted with the FactSage™ thermochemical simulation program. Different conditions were tested to determine the optimum synthesis parameters. MCS was conducted at stoichiometric ratios and different milling durations, using excess reactant amounts over the determined optimum time. After MCS, unwanted phases were removed by HCl acid leaching. Detailed phase analyses of the final powders were obtained by X-ray diffractometer (XRD), whereas detailed microstructure characterization was conducted by scanning electron microscope/energy dispersion spectrometer (SEM/EDS), transmission electron microscope (TEM) and particle size analyzer. Among the utilized parameters, the ideal composition chosen for Mo boride synthesis was 6 h milled and leached MoO_3-100 wt% B_2O_3-50 wt% Mg (1.41 μm), including α-MoB, β-MoB, MoB_2, Mo_2B, Mo_2B_5, and Mo phases. For the synthesis of W boride, the proper composition was found as WO_3-100 wt% B_2O_3-50 wt% Mg (0.37 μm) containing W_2B_5, WB, β-WB, WB_4, W_2B, and W phases after milling for 20 h and leaching. Besides, as a result of the oxidation resistance measurements at 700 and 800 °C, phases belonging to MoO_2 and WO_2 were found along with boride phases.

1. Introduction

Refractory metals have high melting points [1–4], superior chemical resistances, and mechanical properties [5–7], each of which can combine with boron to generate a range of stable compounds [8]. Due to their covalent and metallic bonds, refractory metal borides exhibit outstanding properties such as high corrosion and moderate-temperature resistance [9–11]. Refractory borides such as HfB_2, TiB_2, ZrB_2, TaB_2, NbB_2, etc., stand out widely [8,10–12]. Several processing methods have been utilized for the production of refractory borides. Carbo/borothermal reduction [13–15], molten salt electrolysis [16–18], sol-gel method [19,20], and self-propagating high-temperature synthesis (SHS) [21,22] are some of these methods. Unlike these methods, mechanochemical synthesis (MCS), a room-temperature powder metallurgy technique, is widely preferred in producing refractory borides [23–25]. Ricceri and Matteazzi [26], who are some of the pioneers of boride production by MCS, produced TiB_2 (50–100 nm) at less than 2 h by high-energy ball milling (HEBM) using an 18:1 ball-to-powder weight ratio (BPR) from 1.2 g of powder mixture containing B_2O_3, TiO_2 and Mg, and obtained 81 % process efficiency after leaching. In MCS, particle size reduction and surface area of the particles increase with HEBM, thus increasing their possibility of reacting [27–29]. As a result of cold welding, the structure accumulates many defects with enormous impact energy introduced into the system, and hence the thermodynamic balance is decreased [27,30]. New phases are formed with the chemical reactions that occur by repeated welding and fracturing, and even complex-shaped materials that are difficult to produce can be synthesized at room temperature from cheap starting

* Corresponding author.
** Corresponding author.
E-mail addresses: suzeri@itu.edu.tr (İ. Süzer), bozkurtdu@itu.edu.tr (D. Ağaoğulları).
[1] Equal Contribution.

https://doi.org/10.1016/j.ceramint.2025.02.220
Received 28 November 2024; Received in revised form 28 January 2025; Accepted 15 February 2025
Available online 16 February 2025

materials [31]. It has been emphasized that the new phases formed with MCS may vary due to kinetic and non-equilibrium conditions [23,24]. Although MCS is a process that starts and ends at room temperature, the temperature increases to an uncertain temperature due to long milling durations [24]. Different phases may form from theoretical calculations both as a result of collisions and with a slight increase in temperature. Also, the MCS process can be controlled by many parameters, such as milling duration, BPR, milling speed, milling media, milling atmosphere, process control agent, etc. [32], which affect the quality of the final phases.

Among refractory borides, molybdenum borides (Mo-borides) are superhard materials highly resistant to wear and corrosion. Owing to these properties, they can be used as components in composite materials, machining tools, or coatings [33–35]. Additionally, Mo-borides are preferred in moderate- or high-temperature environments as electrocatalysts for catalytic applications like hydrogen evolution reactions [36–39]. The Mo-B binary system consists of five intermediate main phases: MoB, Mo_2B, MoB_2, Mo_2B_5, and MoB_4. Besides, MoB has two allotropic transformations: α-MoB, a low-temperature phase, and β-MoB, a high-temperature phase. The diboride of Mo, which is a high-temperature phase, exists between ~1800 °C and 2375 °C. Mo_2B, Mo_2B_5, and MoB_4 are formed in the vicinities of approximately 2280 °C, 2140 °C, and 1807 °C, respectively [40]. Çamurlu [41] synthesized MoB from MoO_3, B_2O_3, and Mg starting powders by MCS, HCl leaching, and annealing (1400 °C, 3 h). Although Mo_2B, MoB, MoB_2, and Mo were present in the structure after MCS, they transformed into a single α-MoB phase after annealing. Torabi et al. [42] synthesized Mo boride nanoparticles from MoO_3, B_2O_3, and Mg starting powders by HEBM. A milling time of 4 h was required to obtain Mo boride phases with an average particle size of 100 nm in different stoichiometries. In addition, it was observed that MgO and elemental Mo formed after milling.

Another group of refractory borides, tungsten borides (W-borides), stand out among refractory metal borides with all these features and high electrical and thermal conductivity [2,43,44]. It also pays attention for its use in nuclear applications [45]. It can also be an abrasive-corrosion-resistant electrode material in extreme environmental conditions [46,47]. Apart from this, it has different areas of use, such as being preferred as a composite ceramic material (W_2B, WB, W_2B_5) [48,49]; as a hard coating (WB, W_2B_5, WB_4) [50–52] and as an electrocatalyst (W_2B_5) [53,54]. W_2B, WB, and W_2B_5 are the three nonstoichiometric-intermetallic phases in the W-boride system [55]. Like MoB, WB also shows an allotropic transformation, with the α-WB phase at low temperatures and β-WB at high temperatures [56]. According to the phase diagram, W_2B and W_2B_5 form until the end of approximately 2670 °C and 2365 °C, respectively [55]. To date, several investigations have been carried out to produce W boride. Coşkun and Öveçoğlu [43] synthesized W_2B_5 powders with an average particle size of 226 nm from $WO_{2.72}$, 50 wt% B_2O_3 and Mg starting powders after 30 h of MCS and 7 M HCl leaching. Bahrami-Karkevandi et al. [46] examined the MCS behaviors of W boride-based nanocomposite powders from WO_3-B_2O_3-Mg starting powders by HEBM and leaching (18 % HCl) at different times (20, 60, 360, 540, and 1800 min). They initially found W, W_2B, WB, and MgO phases, but MgO and WB were removed after leaching and milling. As a result, W_2B and W phases were obtained with a particle size of 40–500 nm.

This study synthesized Mo-boride and W-boride powders from MoO_3/B_2O_3/Mg and WO_3/B_2O_3/Mg starting powders by MCS and leaching process. Different experimental parameters were conducted during MCS. First, the optimum duration was determined for the powders synthesized in stoichiometric amounts. Then, production in excess reactant amounts was completed. The formation of phases, reaction temperatures, and product amounts were examined in detail using the thermochemical calculation method. Finally, acid leaching was conducted on the synthesized powders with HCl. Detailed phase analysis, microstructural and physical characterization were conducted on the synthesized and leached powders. As a result, multi-phase Mo-boride and W-boride powders were obtained. Also, this study may aim to bridge that gap by demonstrating the simultaneous production of multiple boride phases at room temperature using MCS, guided by thermochemical calculations. To the best of our knowledge, this work represents a novel approach, offering valuable insights for future research, particularly in cases where the controlled synthesis of mixed boride phases is desired, and hence it will provide significant contribution to the literature. As a result, this study aimed to represent that MCS can yield multiple borides simultaneously at room temperature, as compared to thermochemical calculations.

2. Experimental Procedure

2.1. Thermochemical calculations

Thermochemical calculations were conducted by FactSage™ 7.3 software using “equilib" and "reaction" modules to simulate the governing mechanochemical reaction for Mo-borides (Eq. (1)) and reaction for W-borides (Eq. (2)) concerning varying B_2O_3 and Mg contents between 0 and 14 mol. In the calculations, the "equilib” module was used under 1 atm, 25 °C initial conditions, and it was assumed that reactions take place under adiabatic conditions ($\Delta H = 0$). In other words, the heat energy generated is spent on increasing the temperature of the products with no heat and mass loss to the environment. Under these assumptions, the adiabatic temperatures, stable phases, and compositions were calculated using the FactPS database for the possible gas and compound phases. ΔH and ΔG values were calculated at 25 °C/1 atm in the reaction module.

2.2. Powder processing of borides

Molybdenum oxide (MoO_3, China, 99 % purity, particle size <45μ), boron oxide (B_2O_3, ETİ Mine, 99.5 % purity, average particle size ~ 465 μm) and magnesium (Mg, MME, 99.7 % purity, average particle size ~ 145 μm) were used as starting powders for the synthesis of molybdenum borides. First, stoichiometric blends were calculated as 6 g for each MCS batch. Then, excess amounts of B_2O_3 and Mg were used. All calculations were made according to the theoretical reaction given in Eq. (1) to drive a chemical reaction from a starting powder composition. Starting mixtures and milling durations of the Mo-borides with their sample codes are shown in Table 1. The powder amounts and molar ratios are also given in Table S1. Excess amounts were prepared by changing the B_2O_3 and Mg amounts over 6 g.

$$MoO_3 + B_2O_3 + 6\,Mg = MoB_2 + 6\,MgO\left(\Delta H^{\circ}_{25} = \text{-1550.8 kJ/mol};\ \Delta G^{\circ}_{25} = \text{-1665.6 kJ/mol}\right) \quad (1)$$

Tungsten oxide (WO_3, Alfa Aesar, 99 % purity, particle size <45μ), native B_2O_3, and Mg were used as starting powders in synthesizing of tungsten borides. Like Mo-borides, during the synthesis of W-borides, stoichiometric and excess amounts of powders were prepared according

Table 1
Mo-borides' starting mixtures, milling durations and their corresponding sample codes.

Starting Mixtures	Milling Duration (h)	Sample Codes
MoO_3 - B_2O_3 – Mg	1	Mo_S1
MoO_3 - B_2O_3 – Mg	2	Mo_S2
MoO_3 - B_2O_3 – Mg	4	Mo_S4
MoO_3 - B_2O_3 – Mg	6	Mo_S6
MoO_3 - B_2O_3 – Mg	8	Mo_S8
MoO_3 – 50 wt% B_2O_3 – Mg	6	Mo_50B
MoO_3 – 50 wt% B_2O_3 – 25 wt% Mg	6	Mo_50B-25M
MoO_3 – 50 wt% B_2O_3 – 50 wt% Mg	6	Mo_50B-50M
MoO_3 – 100 wt% B_2O_3 – 25 wt% Mg	6	Mo_100B-25M
MoO_3 – 100 wt% B_2O_3 – 50 wt% Mg	6	Mo_100B-50M

to the theoretical reaction given in Eq. (2), with a total batch of 6 g. Starting mixtures and corresponding sample codes used in W-boride synthesis are given in Table 2. The powder amounts and molar ratios are also given in Table S2. Also, non-milled powders are called as-blended.

$$WO_3 + B_2O_3 + 6\,Mg = WB_2 + 6\,MgO\ \left(\Delta H^{\circ}_{25} = -1127.3\ \mathrm{kJ/mol};\ \Delta G^{\circ}_{25} = -1108.9\ \mathrm{kJ/mol}\right) \quad (2)$$

The MCS and leaching processes have the same steps for both metal borides. Only milling durations differ. Before MCS, the powders were mixed in a Turbula WAB T2C for 2 h. Then, powders were milled in a Spex 8000D Mixer/Miller with a BPR of 10:1. Powders and balls (⌀ 6 mm in diameter, ~1 g each) were placed in the vials (50 ml) under an Argon (Ar, Linde, 99.99 %) atmosphere in an MBRAUN glovebox. Since the powders were prepared based on 6 g, a total of 60 g of balls were added. Both vial and ball materials were hardened steel. Milling durations were selected as 1, 2, 4, 6, and 8 h for Mo borides and 4, 8, 10, 15 and 20 h for W-borides. Mo-borides excess powders were milled for an optimum duration of 6 h, and W-borides excess powders were milled at 20 h. In order to remove unwanted phases, excess amounts of powder were prepared and experiments were carried out on both Mo-borides and W-borides. There are several examples of different studies in the literature [12,23,57].

After milling, stoichiometric and excess blends were purified with 4 M HCl (Merck™, 37 %) leaching. The solution was prepared with a solid-to-liquid ratio of 1 g powder to 10 mL acid. After that, the prepared solution was mixed in a mechanical stirrer for 1 h in the beaker. The liquid acid-powder mixture taken from the beaker was placed opposite each other in four different centrifuge tubes so that their weights were the same. Later, the solution was washed repeatedly with distilled water in a Rotofix centrifuge (4000 cycles/min, 10 min) until it reached a pH of 7. When the centrifuge tubes are taken out of the device, the powders to be synthesized have settled to the bottom, while the unwanted liquid part remains on top. The supernatant liquid was repeatedly decanted. The resulting powders were dried in the stove at 120 °C for 24 h. Then, two compositions (Mo_100B-50M and W_100B-50M) considered to be most suitable for synthesis were selected as representative samples, and oxidation studies were carried out at two different temperatures (700 and 800 °C) at a Protherm tube furnace, in which temperature was increased by 10 °C/min under air and hold for 10 min.

2.3. Characterization studies

The powders' phase analyses were examined under CuK_α radiation (35 kV, 40 mA), the scan rate of 2°/min, and the range of diffraction angles 10–90° with Bruker D8 X-ray diffractometer (XRD). The International Centre for Diffraction Data (ICDD) powder diffraction database was utilized to determine phases. Morphological examinations of the synthesized powders were done via a scanning electron microscope (SEM, JEOL 6000 Neoscope) equipped with an energy dispersive spectrometer (EDS) and transmission electron microscope (TEM, JEOL JEM-2000EX for W-borides and JEOL JEM-ARM200CFEG UHR for Mo-borides). High-resolution (HR) TEM images were also monitored from the analyses. The particle sizes of the synthesized powders were measured using the Microtrac SYNC Laser Diffraction and Dynamic Shape Analyzer and the FLOWSYNC Wet Dispersion Module. Before the measurement, a slurry was created with both samples using Triton 100x, then kept in an ultrasonic bath with water for 5 min. Then, additions were made with a pipette until the laser saturation point was reached. The operation was performed at 60 % motor power, and dispersion was carried out for 3 min with the integrated ultrasonic of the device. The absorbing/irregular calculation method and 1.33 refractive index were used for the liquid in the laser diffraction measurement. A schematic representation of the experimental procedure is shown in Fig. 1.

Table 2
W-borides' starting mixtures, milling durations, and their corresponding sample codes.

Starting Mixtures	Milling Duration (h)	Sample Codes
WO_3 - B_2O_3 – Mg	4	W_S4
WO_3 - B_2O_3 – Mg	8	W_S8
WO_3 - B_2O_3 – Mg	10	W_S10
WO_3 - B_2O_3 – Mg	15	W_S15
WO_3 - B_2O_3 – Mg	20	W_S20
WO_3 – 50 wt% B_2O_3 – Mg	20	W_50B
WO_3 – 100 wt% B_2O_3 - Mg	20	W_100B
WO_3 – 150 wt% B_2O_3 - Mg	20	W_150B
WO_3 – 50 wt% B_2O_3 – 25 wt% Mg	20	W_50B-25M
WO_3 – 50 wt% B_2O_3 – 50 wt% Mg	20	W_50B-50M
WO_3 – 100 wt% B_2O_3 – 25 wt% Mg	20	W_100B-25M
WO_3 – 100 wt% B_2O_3 – 50 wt% Mg	20	W_100B-50M

3. Results & Discussion

3.1. Thermodynamic analysis

Fig. 2a–d shows the thermochemical calculations, such as the effect of the reductant Mg and reactant B_2O_3 contents on the reaction products and the adiabatic temperature of the reactions for the Mo-B system. Fig. 2a demonstrates that the adiabatic temperature increases rapidly with increasing Mg content due to the large exothermicity of the reactions. Lower reductant Mg results in the partial reduction of MoO_3 into MoO_2 and the formation of the MgB_4 phase. For 1 mol of Mg, metallic Mo starts forming at the expense of the MgB_4 phase, which oxidizes into $Mg_2B_2O_5$. Further addition of Mg completes the reduction of MoO_2 into metallic Mo, maximizing at about 3 mol of Mg, accompanied by a maximum in the adiabatic temperature, 2641 °C. The amount of unreduced excess B_2O_3, in the form of the $Mg_3B_2O_6$ phase, decreases at about Mg = 4.5 mol, forming the Mo-rich Mo_2B phase. At the stoichiometric point (Mg = 6 mol), metallic Mo, Mo_2B, MgO, and $Mg_3B_2O_6$ phases are stable. Reductant Mg content needs to be increased beyond the stoichiometric point to synthesize B-rich Mo-B phases. Beyond Mg is 6 mol, and MoB and Mo_2B_5 form. At about Mg equals to 10.5 mol, the $Mg_3B_2O_6$ phase disappears, and 50 % MoB and 50 % Mo_2B_5 product composition are obtained. Further increase in the Mg content results in the formation of the MgB_2 phase, causing the transformation of the B-rich Mo_2B_5 phase into the MoB phase. The T_{ad} value tends to decrease with excess Mg because of the intense gasification of Mg, which decreases the system's temperature. Fig. 2b presents the effect of B_2O_3 content on the phase compositions when Mg content is kept constant at the stoichiometric value and limited B_2O_3 results in forming metallic Mo and Mo-rich Mo_2B phases, as expected. As B_2O_3 increases, the $Mg_3B_2O_6$ phase starts to dominate due to the reaction with MgO peaking at B_2O_3 = 3 mol, where the Mo_2B phase fully transforms into MoB. From this point, the Mo_2B_5 phase appears due to excess boron and stabilizes at B_2O_3 = 8.5 mol, forming a 50 % MoB and 50 % Mo_2B_5 product composition. Further addition of B_2O_3 does not affect the Mo-B phases but forms MgB_4O_7 and B_2O_3 phases. The T_{ad} value tends to decrease from 2473 °C to 1345 °C, because of the less exothermic nature of the reagent mixture. Fig. 2c and d show the effects of the excess B_2O_3 content on the reaction mixtures containing non-stoichiometric Mg (Figs. 2c and 25 wt% excess Mg, Figs. 2d and 50 wt% excess Mg). According to the calculations, increasing both B_2O_3 and Mg increases the boron-rich Mo_2B_5 in the expense of MoB and especially Mo-rich Mo_2B phases, compared to stoichiometric calculation (Fig. 2b).

Thermochemical calculations, including the impact of reactant B_2O_3 and reductant Mg concentrations on the reaction products and the adiabatic temperature of the processes for the W-B system, are depicted in Fig. 3a–d. Similarly, with the addition of reducing Mg into the system, metallic W is a first product at low Mg region accompanied by partially reduced WO_2 and the MgB_4O_7 and $Mg_2B_2O_5$ compounds as given in Fig. 3a for the WO_3-B_2O_3-Mg system. Adiabatic temperature maximizes

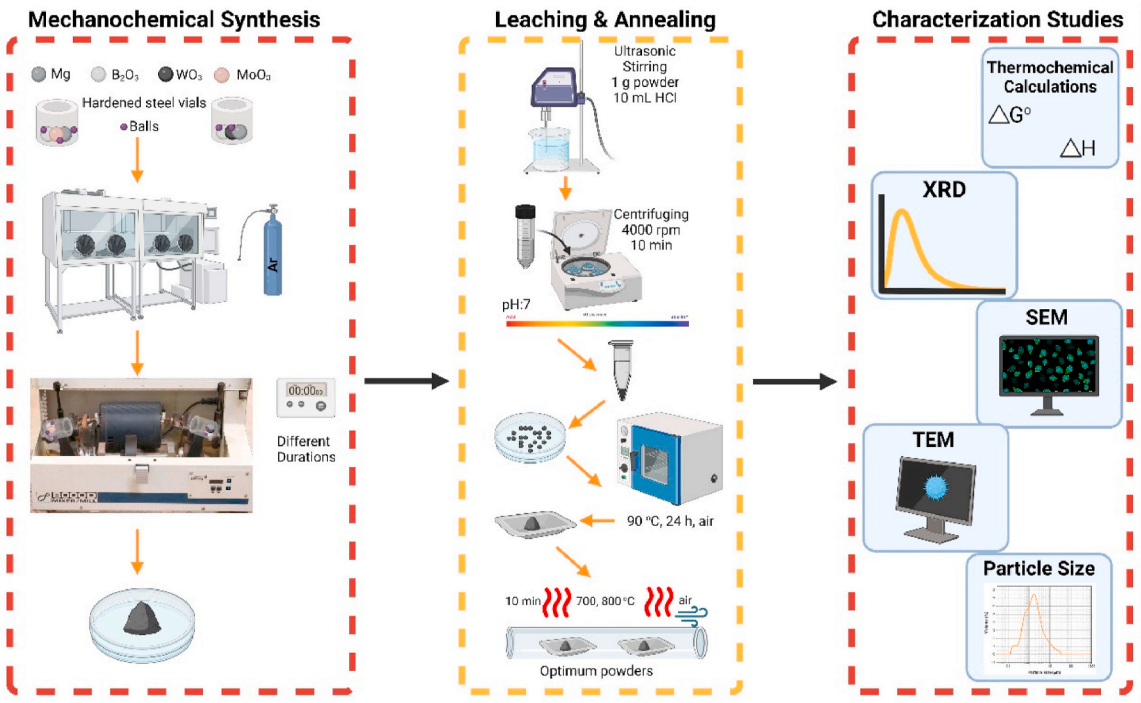

Fig. 1. Schematic representation of the experimental procedure (Created with BioRender.com).

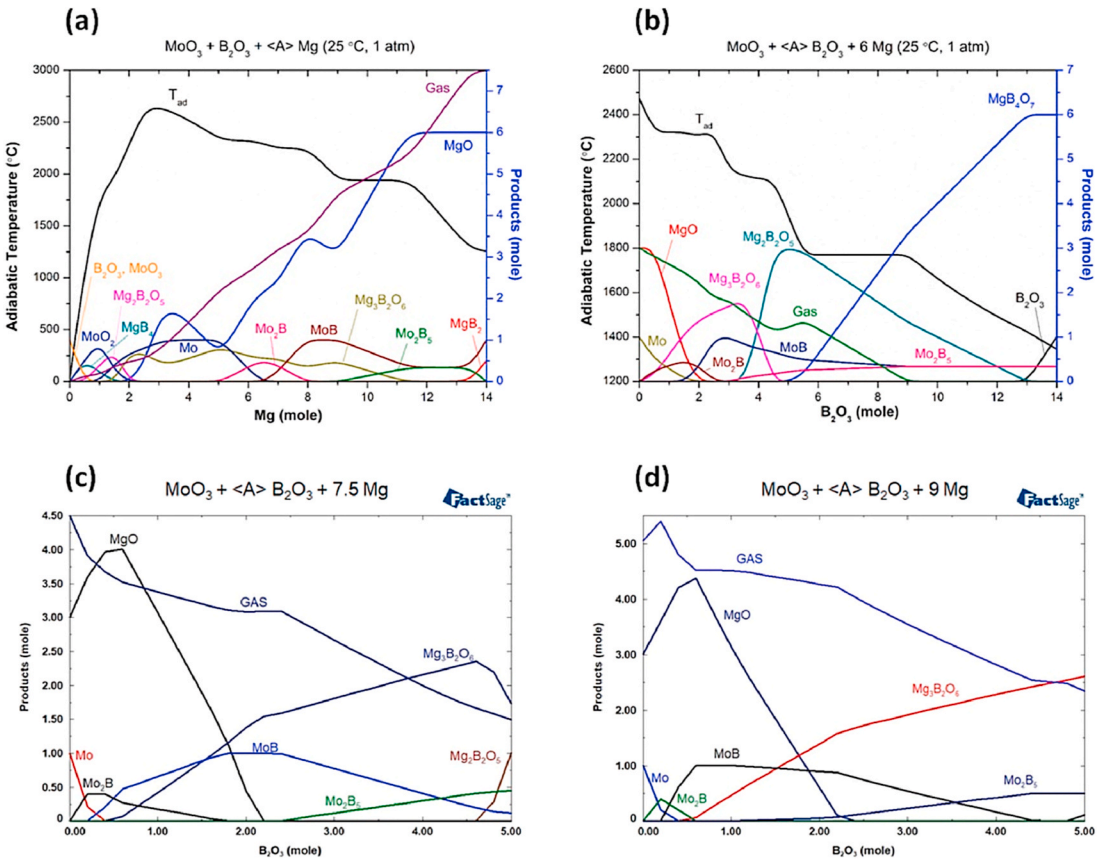

Fig. 2. (a) The effect of reductant Mg content (mol) on the reaction products and the adiabatic temperature of the reagents and products, and the effect of B_2O_3 content (mol) on the reaction products and the adiabatic temperature of the reagents and products for MoO_3-B_2O_3-Mg system in the presence of (b) stoichiometric Mg (6 mol), (c) 25 wt% excess Mg (7.5 mol) and (d) 50 wt% excess Mg (9 mol).

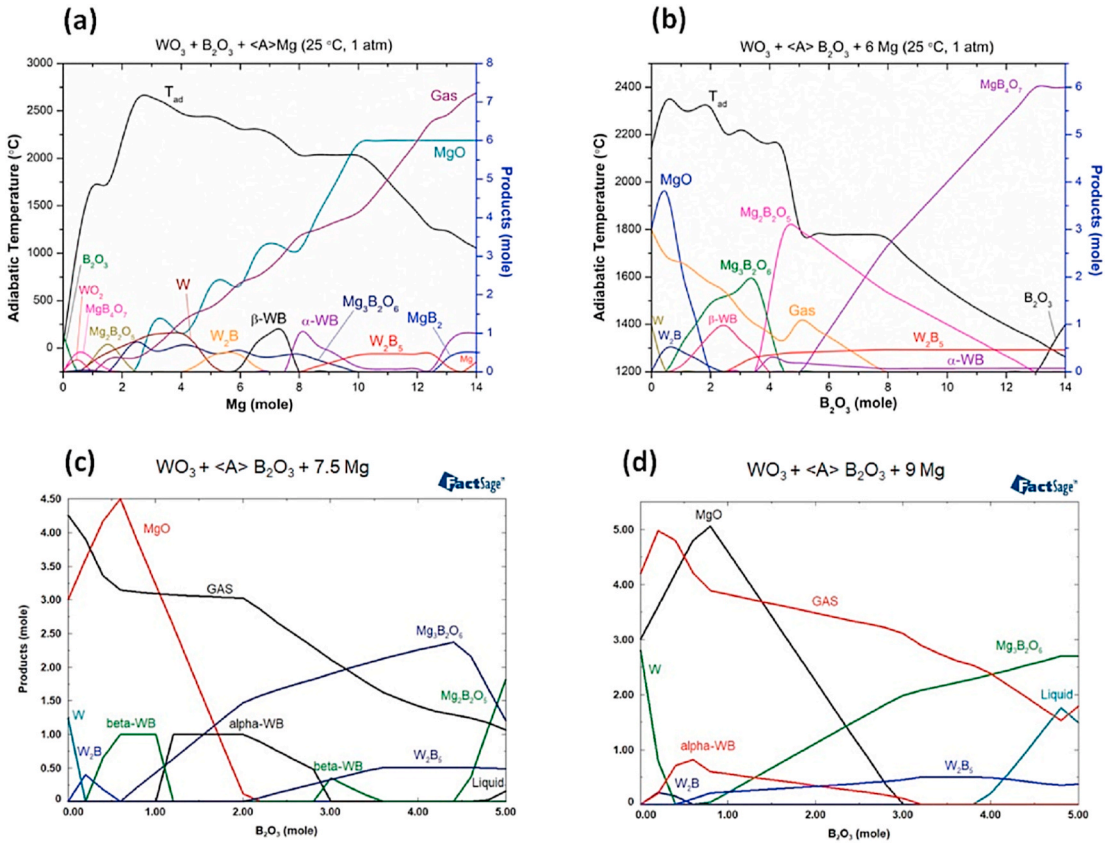

Fig. 3. (a) The effect of reductant Mg content (mol) on the reaction products and the adiabatic temperature of the reagents and products, and the effect of B_2O_3 content (mol) on the reaction products and the adiabatic temperature of the reagents and products for WO_3-B_2O_3-Mg system in the presence of (b) stoichiometric Mg (6 mol), (c) 25 wt% excess Mg (7.5 mol) and (d) 50 wt% excess Mg (9 mol).

at about Mg = 3 mol; however, more Mg is needed to reduce W phase. This boriding process further proceeds with the addition of excess Mg, boron enriched various tungsten borides that form β-WB, α-WB, and W_2B_5 successively. At about 12 mol of Mg, where the $Mg_3B_2O_6$ disappears and W_2B_5 dominates, MgO is the sole reaction product, as expected. Even further addition of Mg leads to the formation of MgB_2 and α-WB phases. The effect of B_2O_3 addition, when Mg is kept constant at 6 mol, is given in Fig. 3b. As expected lower B_2O_3 amounts leads to boron-poor phases, i.e. W, W_2B. As the B_2O_3 increases in the system as the boron source, magnesium borate compounds form where the β-WB phase peaks and adiabatic temperature starts to decrease. Excess B_2O_3 stabilizes the formation of W_2B_5 after the 4 mol of B_2O_3 and a small amount of α-WB phase also accompanies the system in addition to the magnesium borates. Therefore, similar to the MoO_3-B_2O_3-Mg system, increasing the amounts of both B_2O_3 and the Mg reductant relative to stoichiometric ratios (Fig. 3b) leads to the formation of the boron-rich W_2B_5 phase at the expense of W_2B and metallic W. This occurs with a significantly lower B_2O_3 content when 50 wt% excess Mg is used (Fig. 3d), compared to the case with 25 wt % excess Mg (Fig. 3c).

3.2. Characterization of stoichiometric Mo-boride powders

Figs. S1a–d shows the XRD patterns of the raw materials. Figs. S1a, b, and d include only MoO_3 (ICDD: 01-085-2405), WO_3 (ICDD: 00-024-0747), and Mg (ICDD: 00-001-1141) powders, respectively. No by-products, contamination phases, or secondary phases were found. In Fig. S1c, the presence of B_2O_3 (ICDD: 00-044-1085) and H_3BO_3 (ICDD: 00-272-3608) phases are seen due to the moisture in the structure of B_2O_3. The presence of moisture can be reduced by drying&calcining the powders in an oven before the MCS [25]. Additionally, as-blended XRD patterns of the MoO_3-B_2O_3-Mg are shown in Fig. S1e. The XRD pattern (Fig. S1e) consists only of starting powders. The peak intensity of Mg is high, which is expected according to Eq. (1), so Mg peaks dominate over MoO_3 and B_2O_3 peaks. Besides, B_2O_3 is at low intensities due to its amorphous structure. Fig. S1f shows the XRD pattern of the as-blended WO_3-B_2O_3-Mg powders. Similar to Fig. S1e, only the phases of the starting powders can be observed. Also, there is no by-product formation. The most substantial peaks again belong to Mg, which, in this case, causes the peaks belonging to WO_3 to be suppressed.

Fig. 4a is the XRD patterns of MoO_3-B_2O_3-Mg starting powders after milling at different durations (1, 2, 4, 6, 8 h), revealing α-MoB (ICDD: 00-051-0940), β-MoB (ICDD: 00-006-0644), Mo_2B (ICDD: 01-089-1990), MoB_2 (ICDD: 01-089-5152) phases. According to Eq. (1), the MgO (ICDD: 03-065-0476) phase formed as expected. The most intense peak belongs to elemental Mo (ICDD: 01-089-5023). Although the MoB_2 phase is stable above 1500 °C, this phase can be obtained at room temperature with MCS, as stated in the literature [58]. As indicated in the XRD pattern of reactant B_2O_3, an amount of H_3BO_3 is present in the powder structure. The Mo phase detection is related to this moisture absorbed by the B_2O_3 powder. No significant differences were observed during the transition from Mo_S1 to Mo_S2. There are no significant differences in peak intensities in other compositions. Also, MoB_2 is not the primary phase as given in Eq. (1). FactSage™ plot shown in Fig. 4c represents the relation between the reaction products and the increasing amount of H_3BO_3 in the B_2O_3 microstructure. According to this plot, it is evident that the presence of up to 0.4 mol of H_3BO_3 in B_2O_3 leads to an increased amount of elemental Mo. This is due to its negative impact on the reduction mechanism, attributed to the moisture, and its role in reducing the boron content of the B_2O_3 source. This finding was formerly reported in a similar study about the synthesizing of refractory boride via the SHS method [59]. In addition, Fig. 4b shows the XRD patterns of MoO_3-B_2O_3-Mg starting powders after leaching at different

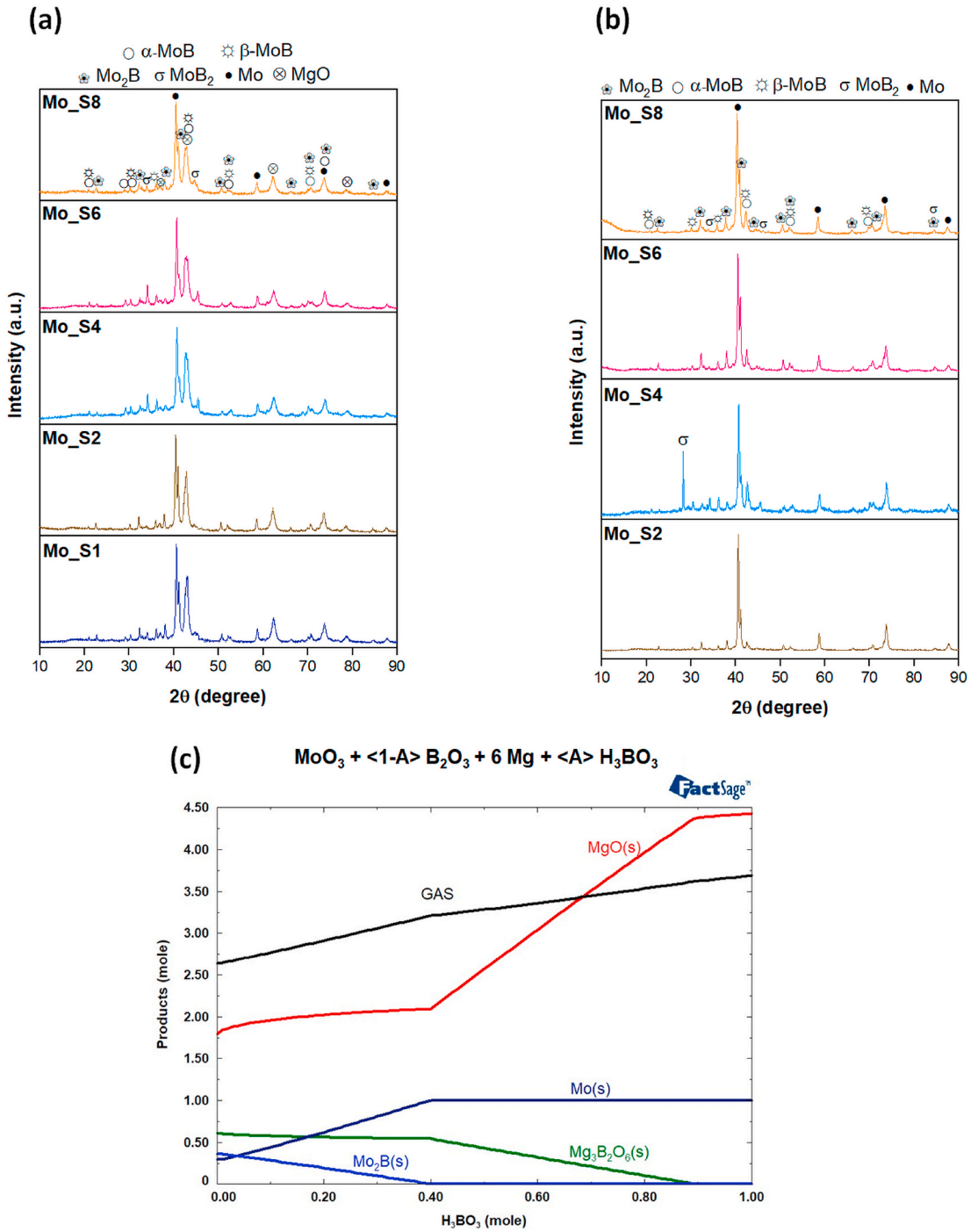

Fig. 4. XRD patterns of stoichiometric MoO_3-B_2O_3-Mg powders (a) after milling and (b) after leaching for different durations (1, 2, 4, 6, and 8 h) and (c) the effect of probable H_3BO_3 in the microstructure of B_2O_3 on the reaction product.

durations (2, 4, 6, 8 h). After HCl acid leaching, MgO was totally removed from the structure. On the other hand, Mo still has the highest intensity. Additionally, MoB_2 appeared only in Mo_S4 but not in other samples with other durations. Besides, α-MoB, β-MoB, and Mo_2B phases also formed. Rybkovskiy et al. [33] stated that the stable phases are α-MoB, MoB_2, and MoB_5. However, they also observed that the formation energy of the β-MoB was higher than that of the α-MoB. Also, elemental Mo has been found in many studies [34,35,41,60,61]. In the C + Mg + MoO_3 system studies carried out so far [62,63], it has been observed that the reduction from MoO_3 to Mo occurs in two steps under appropriate thermodynamic conditions. However, Torabi et al. [64] observed that due to MCS of MoO_3+Mg, the multi-step process was reduced to a single step. The rapid MCS process enabled the conversion of MoO_3 into Mo in a single step in the presence of the Mg reductant. It was suggested that the high melting temperature of Mo and the slow diffusion between Mo and B cause incomplete solid-state reactions and enable elemental Mo to remain in the structure [41].

3.3. Characterization of stoichiometric W-boride powders

Fig. 5a show the XRD patterns of WO_3-B_2O_3-Mg starting powders after 4, 8, 10, 15, and 20 h of milling. Since experiments were carried out between 8 and 24 h in the previous studies [2,43], high milling durations were tried to obtain W-boride. Although the results of short milling

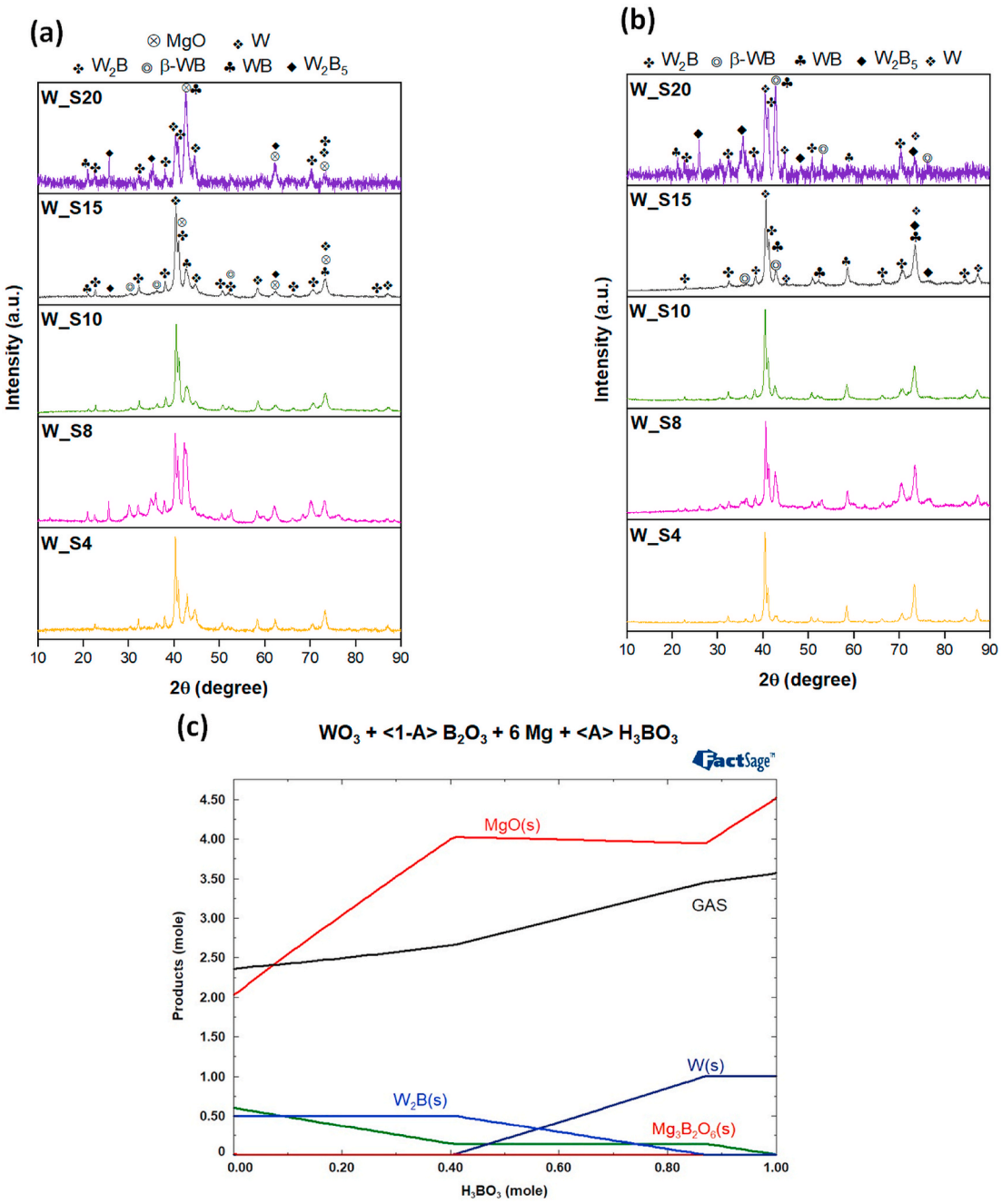

Fig. 5. XRD patterns of stoichiometric WO_3-B_2O_3-Mg powders (a) after milling and (b) after leaching for different durations (4, 8, 10, 15 and 20 h) and (c) the effect of probable H_3BO_3 in the microstructure of B_2O_3 on the reaction products.

times were desired to be seen here, 20 h was chosen as the optimum processing duration. As expected, the MgO phase is present in all compositions. However, elemental W (ICDD: 00-001-1204) also occurred in different 2θ positions. Multi-phase W-borides such as W_2B (ICDD: 01-073-1767), β-WB (ICDD: 00-006-0541), WB (ICDD: 01-073-1769), and W_2B_5 (ICDD: 00-031-1407) formed. According to Fig. 5a, the peak intensity of the MgO phase increased as the milling time increased. However, when the milling time increased, especially after 20 h, β-WB or W_2B phases were removed from the structure. The study by Bahrami-Karkevandi et al. [46] observed that the WB phase completely disappeared after 60 min of milling. The peak intensity of the W phase increased up to 15 h, but decreased after 15 h. After leaching (Fig. 5b), the MgO was removed entirely. This shows that the leaching process was successful. As in the previous sample study [46], the WB phase completely disappeared when the milling time increased. There is elemental W with high peak intensities. In addition, as a result of 20 h of milling and leaching, W_2B and W_2B_5 are found to be the dominant boride phases. Fig. 5c illustrates a FactSage™ plot showing the relation between an increasing amount of H_3BO_3 in the B_2O_3 microstructure and the reaction products: the emergence of the W phase, similar to Mo, can be attributed to the decrease in the available B content and negative contribution to reduction mechanisms by the effect of moisture. The formation of the WB_2, which has a stable structure, was not observed. In a different study conducted with SHS, multi-phase W-borides and elemental W were formed [57]. In another study using HEBM starting from elemental W and B; WB_2, and W occurred [65]. Additionally, as the milling time increased, the intensity of the peaks decreased, and amorphization started. Continuous deformation, crystallite refinement,

and absorbed mechanical energy may cause peak changes [2,46]. Similar situations also emerged after leaching XRD patterns in Fig. 5b. More than one W-boride phase is present in the structure. Here, it can be seen that only MgO has been completely removed from the structure. However, elemental W is still present with high intensity. It is expected that unwanted phases, such as MgO, will be removed by HCl acid leaching. However, products with high chemical stability may remain in the structure, albeit in low amounts. Jalaly et al. [66] produced ZrB_2 from ZrO_2-B_2O_3-Mg starting materials by MCS. Although they observed that the MgO was completely removed after HCl leaching following to milling, the stable ZrO_2 remained.

Based on the characterization studies, 6 h and 20 h were determined as the optimum duration for stoichiometric amounts of Mo-boride and W-boride, respectively. The insufficient use of the boron source (B_2O_3) and/or the reducing agent (Mg) may be the reason for the elemental Mo and W. This indicates that the milling time needs to be increased and more effective when using stoichiometric amounts. For this reason, considering the different studies carried out before, excess amounts (more than the stoichiometric ratio) were used, and it was observed whether there was a change in the composition [23,24,67].

3.4. Characterization of excess Mo-boride powders

In Fig. 6a and b, the XRD patterns of the MoO_3-B_2O_3-Mg starting powders prepared in excess amounts, milled and leached, are given, respectively. When the XRD patterns before leaching were examined (Fig. 6a), only the addition of boron oxide (Mo_50B) showed no difference from the stoichiometric amounts (Fig. 4a). Accordingly, the amount of boron oxide was increased by weight along with Mg. MoB_2, Mo_2B, and α-and β-MoB phases were formed here, similar to stoichiometric amounts. Also, a low amount of MoB_4 (ICDD: 00-020-1235) is formed. As expected, Mo-borides were synthesized in multi-phase. MgO, the by-product, has high intensity. It is also found in elemental Mo in all compositions. However, here, the peak intensity of elemental Mo decreased considerably compared to stoichiometric amounts (Fig. 4a and b). When the XRD patterns after leaching are examined (Fig. 6b), it is seen that MoB_4 is no longer present in the structure. MoB_2, Mo_2B, and α-and β-MoB phases are formed. In cases where B_2O_3 is more than Mg in moles (Mo_50B-25M, Mo_100B-25M, Mo_100B-50M), the boron-rich Mo_2B_5 (ICDD: 00-006-0228) phase was observed. In this case, it can be said that Mg is not sufficient for reduction. Elemental Mo is also present in the structure, although it has low intensities. In Çamurlu's study [41], different Mo-borides and elemental Mo were found after leaching. Yeh and Hsu [60] found that MoB_4 can transform into Mo_2B_5. They said that MoO_3, Mo, and B could not react to form MoB_4, and Mo_2B_5 was the dominant phase. However, in the FactSage™ graphs from Fig. 2a–d, Mo_2B, Mo, MoB, and Mo_2B_5 phases formed according to the changing amounts of Mg or B_2O_3. Fig. 6c shows the Rietveld analysis result of the after-leaching powders. As is known, the Rietveld analysis is a semi-quantitative method. Therefore, the results obtained by Rietveld analysis show approximate weight percentages. This method also confirmed the formation of different boride phases. The Rietveld fitting plots are given in also Fig. S2. Here, it is seen that Mo decreases in weight with each increasing excess composition, and even in Mo_100B-50M composition, it is below 0.5 wt%. Furthermore, MoB_2 is the most intense and dominant phase in all compositions. Mo_2B_5, on the other hand, has a trend of increasing weight as excess amounts in the composition increase. While Mo_2B has a very high amount in Mo_50B-50M, this amount has decreased below 2 wt% in Mo_100B-50M. The fact that elemental Mo has the lowest amount in Mo_100B-50M also qualifies as the selected composition correct for seeing different boride phases. Again, the transformation of the phases depending on the excess amounts is also evident.

Fig. 7a show SEM images of the milled and leached Mo_100B-50M powders. Agglomerated powders with irregular shapes and different sizes were produced. It is known that cold welding causes the formation of agglomerated structures in powders during milling [25]. Additionally, powders are produced at submicron sizes. Again, in studies conducted with MCS, it was found that Mo and W-boride powders with clustered agglomerated structures in submicron sizes were produced [2,

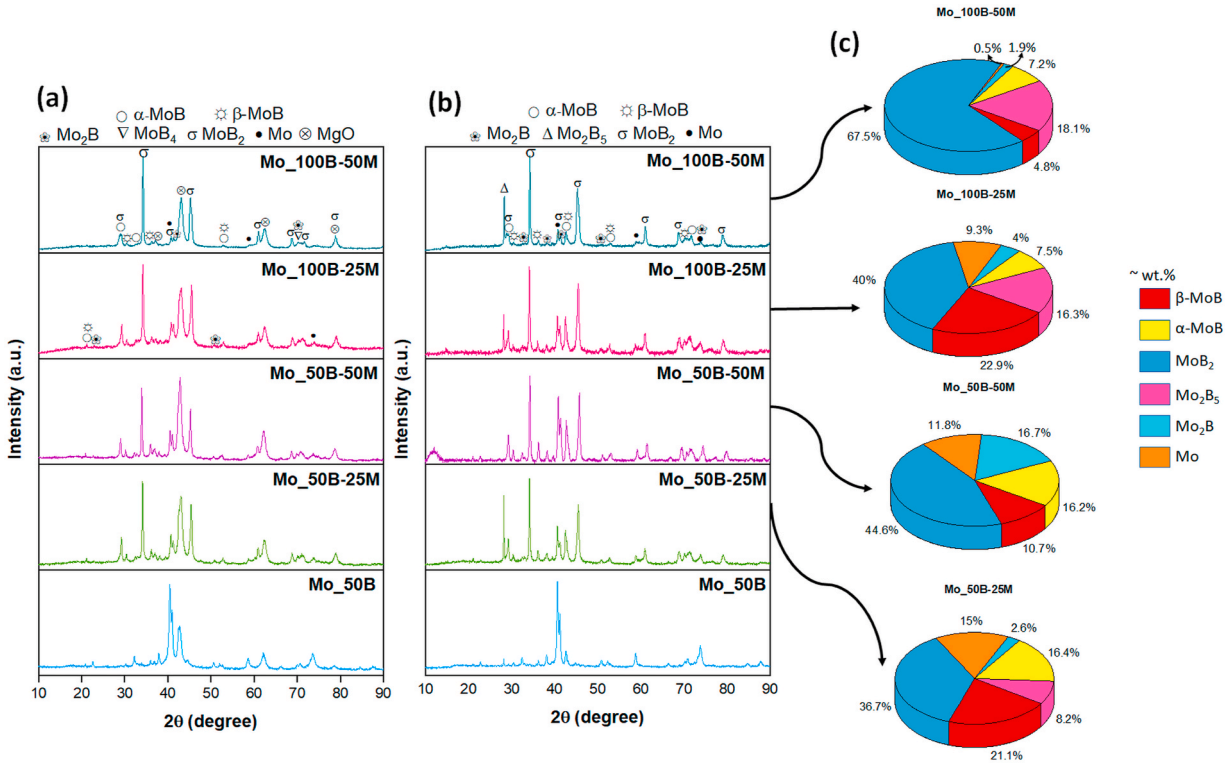

Fig. 6. XRD patterns of Mo_3-B_2O_3-Mg powders containing excess amounts of B_2O_3 and Mg by weight, milled for (a) 6 h, (b) leached, and (c) Rietveld analysis.

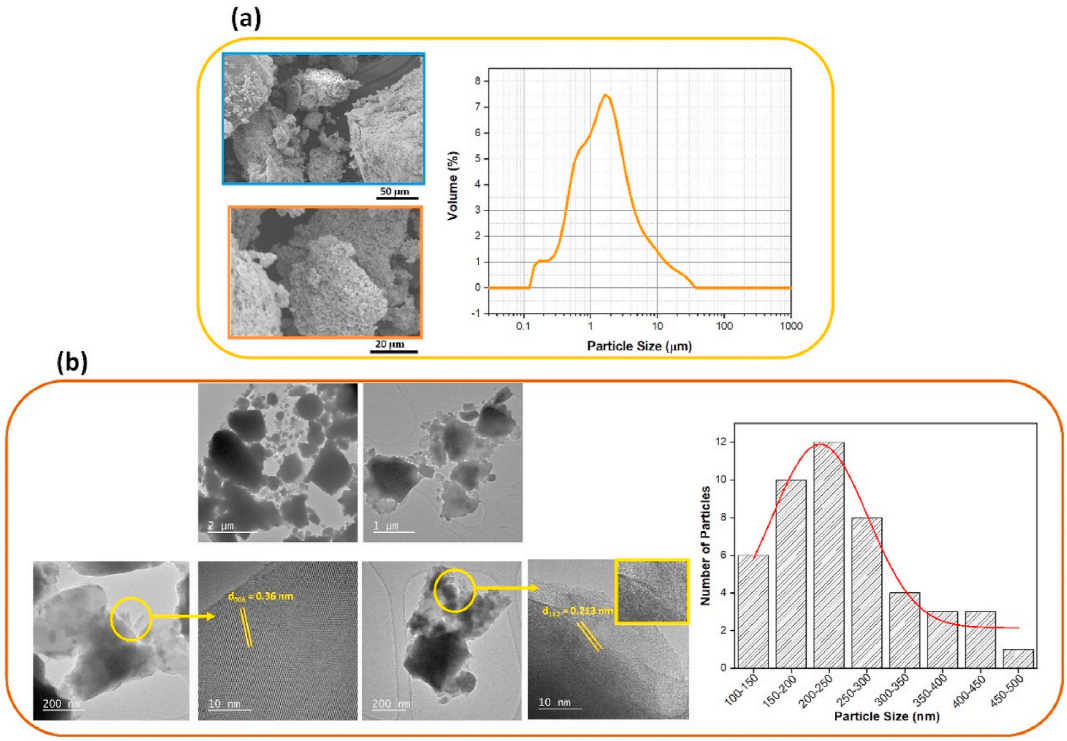

Fig. 7. (a) SEM images and particle size distribution and (b) TEM/HR-TEM images and number of particles versus particle size histogram of the Mo_100B-50M powders.

41–43,46,65]. Fig. 7b contains detailed TEM and HR-TEM images of the leached Mo_100B-50M powders. It can be understood from the TEM images that the powders have irregular structures and mixed shapes. The HR-TEM image the distance between the {006} planes of the Mo_2B_5 phase was measured as 0.36 nm. On the other hand, the distance of the {112} planes were measured as 0.213 nm, which was determined to belong to the α-MoB phase. The Mo_2B_5 phase occurs according to the XRD patterns and is expected to be included in HR-TEM images. In addition, this detected phase confirms that the synthesis has taken place successfully and that characterization results complement each other. Fig. 7a also shows the particle size distribution (PSD) of the Mo_100B-50M powders. The 50 % of the powders are 1.41 μm and

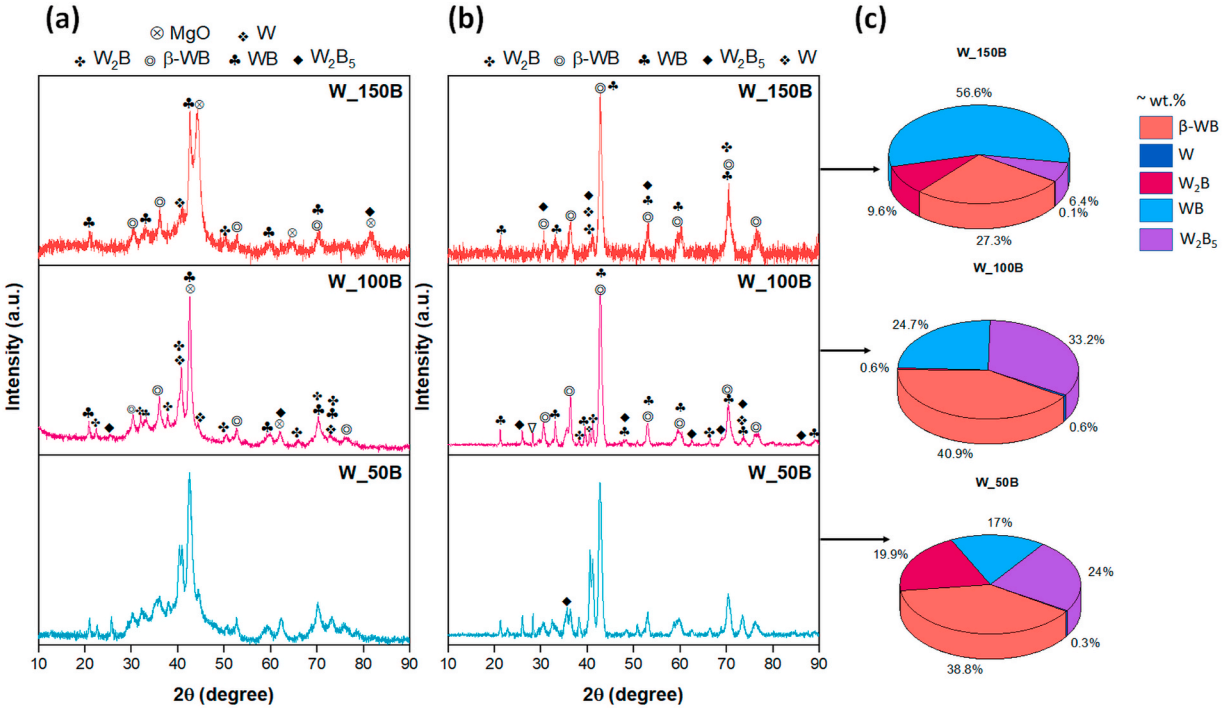

Fig. 8. XRD patterns of WO_3-B_2O_3-Mg powders containing excess amounts of B_2O_3 (50, 100, and 150 wt%) (a) milled for 20 h, (b) those leached and (c) their corresponding Rietveld analysis.

below. However, it is understood that the PSD is in a wide range from 0.4 μm to 19 μm. During the PSD, the particle sizes of the dissolved powders are measured. In addition, particle images and heat map during PSD measurement are given in Figs. S4a–b. According to Fig. S4a, particle images are sorted from largest to smallest and do not represent the entire sample. According to the heat map in Fig. S4b, the horizontal axis shows the equivalent circle diameter, and the vertical axis shows the aspect ratio. Color values change according to the volume ratio that the particles cumulatively occupy in the measured volume. In Fig. 7b, the PSD of the particles seen in TEM and the measured particle numbers are given. It should be remembered that TEM examines a small and specific area and provides information about the sizes of the particles in this area. It does not include the PSD distribution of the produced powders.

3.5. Characterization of excess W-boride powders

Besides all these, another study showed that as the B_2O_3 ratio increased, the W, W_2B, and MgO phases decreased [57]. For this reason, the B_2O_3 ratio was increased in this study. Fig. 8a show the XRD patterns of WO_3-B_2O_3-Mg starting powders that were milled for 20 h and contained 50, 100, and 150 wt% excess B_2O_3. Coşkun and Öveçoğlu [68] stated in their study that it is challenging to form W-borides under 20 h. However, to observe the change in boride formation with the change of rpm amount, different times were tried, and again, 20 h was selected as the optimum. Like the stoichiometric amounts of W-borides (Fig. 5a), W, W_2B, β-WB, WB, and W_2B_5 occurred in all compositions. As expected, MgO is also present in the peaks after milling. Fig. 8b shows the XRD patterns after leaching. MgO has been completely removed from the structure. β-WB and WB emerge as the dominant phase. In addition, low-intensity W_2B and W_2B_5 formation is also observed. In addition, although the peaks belonging to elemental W in the W_100B composition have quite high intensity, the intensity of these peaks in the W_150B composition has decreased to almost none. Like in the Mo boride synthesis (Fig. 6), elemental W could not be removed. Later, since it has a high melting point, it cannot undergo the desired reactions and remains in the structure [46,69]. Additionally, MgO can be removed by leaching, while W remains present in the structure because it has very low solubility in HCl [43,69]. However, in the W_150B, the phases started to become amorphous, the peak widths increased, and accordingly, tungsten boride phases were not seen. Therefore, it has been observed that simply increasing B_2O_3 in excess amounts does not contribute significantly. Moreover, W, WB, W_2B, and W_2B_5 were produced in different studies using excess amounts of B_2O_3 [2,59,69]. Fig. 8c shows the Rietveld analysis results of the post-leaching powders. Like the Mo-borides (Fig. 6c), there are overlapping and low-intensity peaks here. As a result, these results are approximately weight percentages. Elemental W amounts are below 1 wt%. It is seen that α and β-WB phases are more than the others. W_2B and W_2B_5 amounts have very low percentages in the W_150B composition.

The XRD patterns of the compositions milled for 20 h and leached containing excess amounts of B_2O_3 and Mg are shown in Fig. 9a and b, respectively. The Rietveld fitting plots are given in also Fig. S3. WB, β-WB, W_2B_5, and W_2B phases, along with low-intensity W and MgO phases, were observed in the XRD patterns after milling (Fig. 9a). In their study, Bahrami-Karkevandi et al. [46] obtained W_2B and W phases after leaching. No boride phase was formed after leaching in a different study, and elemental W remained in the structure [57]. As the excess amount changed, phase transformations occurred, the intensities of the peaks changed, and amorphization was also observed in some phases. MgO was removed entirely in the after-leaching XRD patterns (Fig. 9b). WB_4 (ICDD: 00-031-1407) formation has also begun to be observed. There is elemental W with a very low peak intensity. The dominant phase belongs to W_2B_5 in all compositions. In a study conducted with SHS, it was observed that when excess B_2O_3 was used, the reaction for reduction with Mg occurred more quickly, and as a result, debt-rich W_2B_5 phases were formed. In excess amount of B_2O_3, the WO_3 phase is surrounded by B_2O_3. As a result, boron is formed around W particles, and a boron-rich phase is obtained [69]. On the other hand, different phases predominate in stoichiometric amounts and excess amounts. Due to the reaction stoichiometry, another study showed that W_2B_5 was dominant in excess cases instead of WB [2]. The study by Bahrami-Karkevandi et al. [46] stated that the WB decreased or even disappeared with increasing milling time. In other words, in the graphs showing the phases depending on the amounts of Mg and B_2O_3 varying

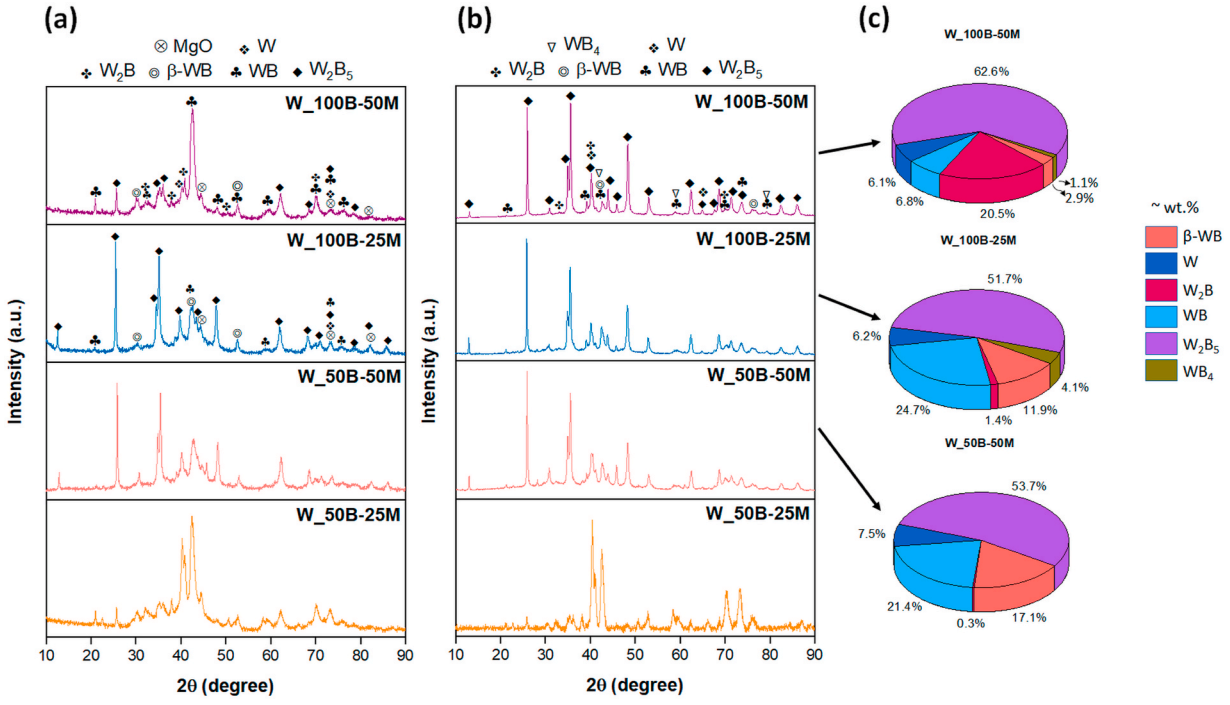

Fig. 9. XRD patterns of WO_3-B_2O_3-Mg powders containing excess amounts of B_2O_3 (50 and 100 wt%) and Mg (25 and 50 wt%) (a) milled for 20 h, (b) those leached and (c) their corresponding Rietveld analysis.

with FactSage™ (Fig. 3a–d), it is seen that different W-boride phases are formed (W_2B_5, α-WB, β-WB, W_2B, W). Changing thermodynamic conditions during MA may also cause variability in phases. Fig. 9c shows the Rietveld analysis results of the after-leaching powders. Similar to previous results, the values are given as approximate weight percentages. In addition, elemental W decreased below 2 wt% in the W_100B-50M composition. WB_4 was formed in very low amounts. All phases except W_2B_5 decreased towards W_100B-50M. When all Rietveld analysis results are examined together, it is seen that elemental Mo or W gradually decreases in the use of excess amounts. In this way, synthesizing the desired boride phases together will be completed.

Fig. 10a shows the SEM images of the milled and leached W_100B-50M powders with irregular shapes and different sizes like Mo-borides. Fig. 10b contains TEM and HR-TEM images of leached W_100B-50M powders. Particles with mixed shapes and needle structures are seen in the composition. According to the HRTEM image in Fig. 10b, the phase located in the {012} plane and with an interplane distance of 0.253 nm belongs to W_2B_5. This also confirms the XRD pattern. Fig. 10a shows the PSD of the W_100B-50M powders. The 50 % of the synthesized powders are 0.37 μm and below. The general distribution is between approximately 0.1 μm and 7 μm. Similar to Mo-boride powders, particle images and heat map are included in Figs. S5a–b. The particle images in Fig. S5a do not represent the entire sample, as they are sorted from largest to smallest. It is also understood that the particles in the heat map in Fig. S5b are distributed in a wider area than Mo-boride. Fig. 10b shows the PSD and corresponding particle numbers obtained from TEM images. Just like in Mo-boride powders (Fig. 7b), it should be noted that TEM takes measurements from a specific and smaller area. In addition, the main purpose of TEM images is to detect phases and to comment on particles and their shapes rather than determining particle size. In addition to all these, it should be remembered that powders have an agglomerated structure, and failure to distribute this structure homogeneously may also affect PSD.

In Fig. 11a and b, the oxidation resistances formed by heating the selected compositions (Mo_100B-50M and W-100B-50M, respectively) to different temperatures (700, 800 °C) were investigated. According to Fig. 11a, different Mo-boride phases (α-MoB, β-MoB, Mo_2B, MoB_2) emerged with elemental Mo after heating. However, it is seen that the MoO_2 (ICDD: 00-002-0422) phase also formed. The oxidation graphs drawn with FactSage™ at 700 and 800 °C are given in Fig. 11c. Here, it is seen that Mo_2B_5, Mo_2B, MoB, and Mo phases will be formed depending on the amount of oxygen. In addition, it is understood that both MoO_2 and MoO_3 are formed at 3.5 and 6.5 mol of O_2, respectively, and that MoO_3 will remain in the stable phase as oxygen increases. In addition, another study has stated that MoB can be oxidized to MoO_2 or MoO_3 at 600 °C [70], and these two phases can form because they have different Gibbs free energy changes. In Fig. 11b, along with different W-boride phases (W_2B, WB, W_2B_5), elemental W and WO_2 (ICDD: 01-082-0728) are also formed. Here, oxidation is higher than Mo-boride. Soylu et al. [71] also emphasized that α- and β-WB would be easier to be oxidized towards WO_3. According to the oxidation graphs in Fig. 11d, drawn with FactSage™ at 800 °C, different W boride phases and elemental W are expected to be formed. However, WO_2 and WO_3 are also formed. It can be said that the WB phase may also start to oxidize at 600 °C; however,

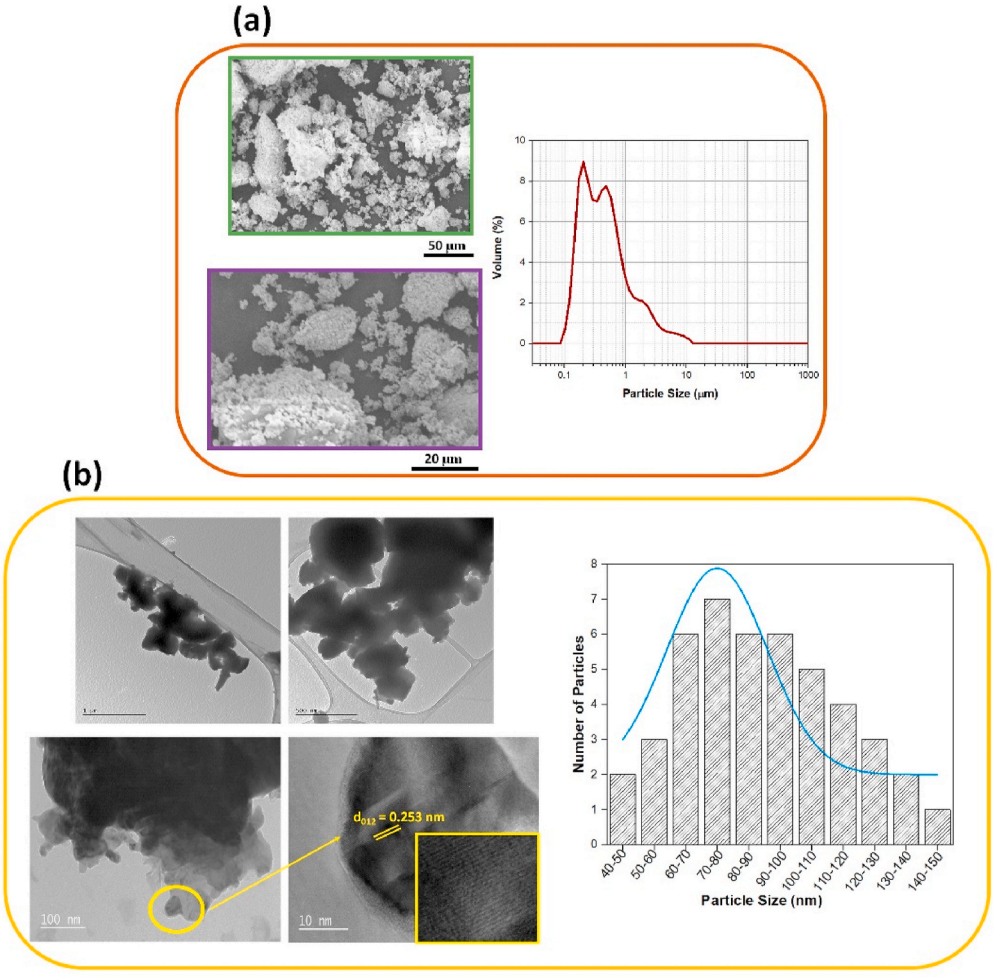

Fig. 10. (a) SEM images and particle size distribution and (b) TEM images and number of particles versus particle size histogram of the W_100B-50M powders.

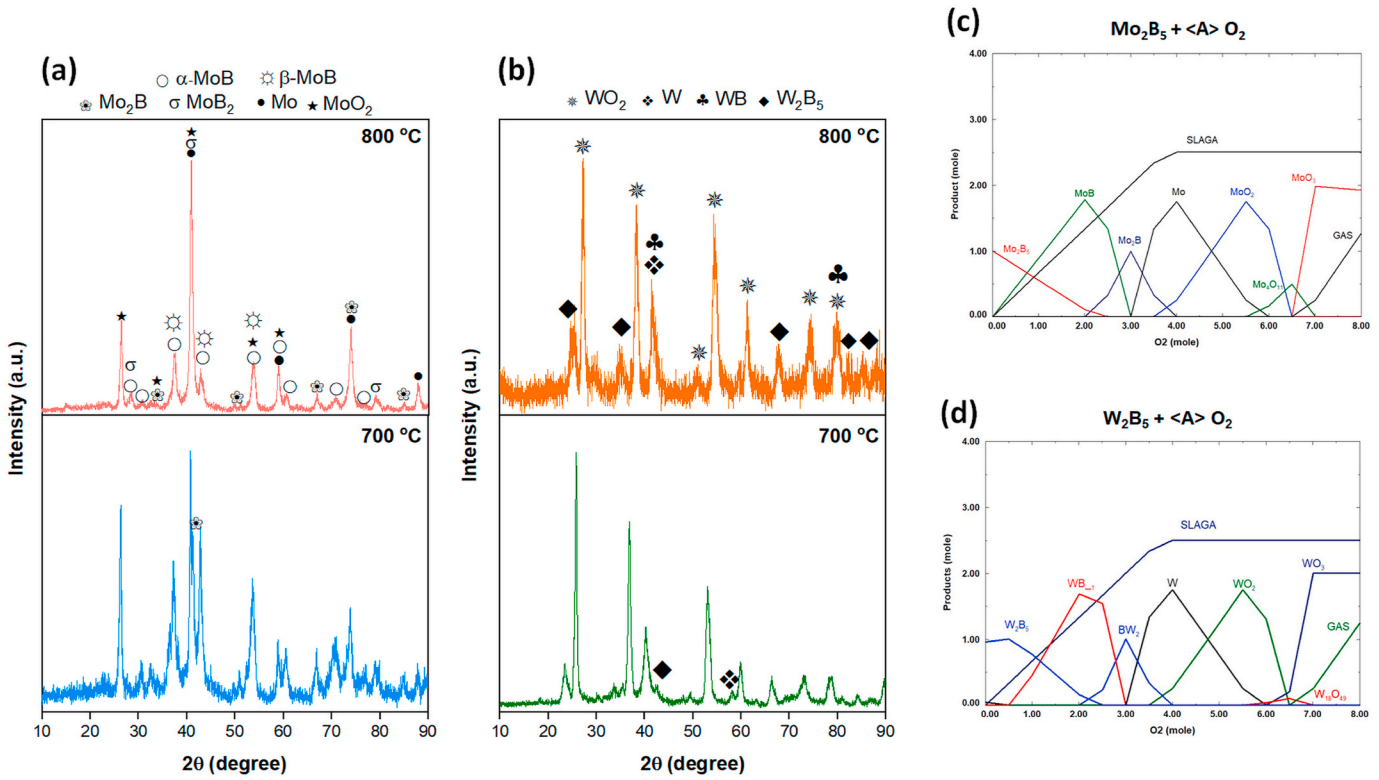

Fig. 11. Oxidation studies at different temperatures (700, 800 °C): (a–c) Mo-borides, and (b–d) W-borides.

when the boron amount increases to 50 %, the oxidized layer thickness increases, and it oxidizes even more with increasing temperature [72]. For the oxidation of Mo and W-borides, an amount of elemental Mo and W emerged in the powder due to the reaction of B and O_2 and, later, the volatilization of B_2O_3. Here, it can be seen that W-borides oxidize more quickly, and in this case, their oxidation resistance may be weaker than Mo-borides.

Table 3 shows the phases of the composition of Mo-boride milled and leached for 6 h and W-boride milled and leached for 20 h. Different boride phases are formed along with elemental Mo and W. Also, a few studies in the literature involve the synthesis of Mo-boride and W-boride by using MCS. Some studies in the literature include the synthesis of Mo-boride and W-boride separately [35,57,60,69,73,74]. However, synthesis with MCS is quite rare [42,43,46]. In addition, these studies could be carried out to yield single or two-phase products [34,35,43,46,69]. This study synthesized the stable phases seen in the phase diagrams and the phases expected to occur due to thermochemical calculations. Although it is difficult to see all the phases at the same time, the production of different borides together was successfully achieved at room temperature.

Table 3
Final phases of the compositions.

Sample	Phases
Mo_50B-25M	β-MoB, α-MoB, MoB_2, Mo_2B_5, Mo_2B, Mo
Mo_50B-50M	β-MoB, α-MoB, MoB_2, Mo_2B, Mo
Mo_100B-25M	β-MoB, α-MoB, MoB_2, Mo_2B_5, Mo_2B, Mo
Mo_100B-50M	β-MoB, α-MoB, MoB_2, Mo_2B_5, Mo_2B, Mo
W_50B	β-WB, W_2B_5, WB, W_2B, W
W_100B	β-WB, W_2B_5, WB, W_2B, W
W_150B	β-WB, W_2B_5, WB, W_2B, W
W_50B-50M	W_2B_5, W, WB, W_2B, β-WB
W_100B-25M	W_2B_5, W, WB, W_2B, β-WB, WB_4
W_100B-50M	W_2B_5, W, WB, W_2B, β-WB, WB_4

4. Conclusions

In this study, multi-phase Mo-boride and W-boride powders were synthesized from $MoO_3/B_2O_3/Mg$ and $WO_3/B_2O_3/Mg$ starting powders by MCS and HCl acid leaching. Refractory borides have been successfully produced under different synthesis parameters. These production results have been demonstrated both experimentally and theoretically. Based on the results of the present study, the following conclusions can be drawn:

- MoO_3-B_2O_3-Mg starting powders prepared in stoichiometric amounts were milled for 2, 4, 6, and 8 h. After milling and leaching, α-MoB, β-MoB, Mo_2B, MoB_2, Mo_2B_5, and Mo phases formed.
- WO_3-B_2O_3-Mg starting powders prepared in stoichiometric amounts were milled for 4, 8, 10, 15 and 20 h. After milling and leaching, W_2B_5, WB, β-WB, WB_4, W_2B, and W phases formed.
- MoO_3-B_2O_3-Mg, prepared in excess amounts, was initially milled for 6 h. After milling and leaching, α-MoB, β-MoB, Mo_2B, Mo_2B_5, MoB_2, and Mo phases formed.
- WO_3-B_2O_3-Mg starting powders prepared in excess amounts were milled for 20 h. After milling and leaching, W_2B_5, WB, β-WB, WB_4, W_2B, and W phases occurred.
- Average particle sizes, SEM, and TEM images are presented for each representatively selected composition. Mo_100B-50M powders have an average size of 1.41 μm, while W_100B-50M powders have a size of 0.37 μm.
- α-MoB, Mo_2B_5, and W_2B_5 phases were found in the HR-TEM images.

CRediT authorship contribution statement

İlayda Süzer: Writing – original draft, Methodology, Investigation, Data curation, Conceptualization. **Amir Akbari:** Writing – original draft, Methodology. **Faruk Kaya:** Writing – original draft, Software. **Sıddıka Mertdinç-Ülküseven:** Writing – original draft, Methodology, Investigation. **Bora Derin:** Writing – original draft, Software. **M. Lütfi**

Öveçoğlu: Writing – review & editing. **Duygu Ağaoğulları:** Writing – review & editing, Writing – original draft, Supervision, Project administration.

Declaration of competing interest

The authors declare that they have no known competing financial interests or personal relationships that could have appeared to influence the work reported in this paper.

Acknowledgment

This study was financially supported by the "TENMAK Boron Research Institute (BOREN), Türkiye" with the project number of 2019–31-07-15-001. It was also partially funded by the Istanbul Technical University Scientific Research Projects (ITU-BAP) with the project number of MDK-2022-43573. The authors also thank M.Sc. Esin Aysel for her help during the experimental studies, Özgür Duygulu, PhD for TEM analysis and ATS (Advanced Technological Solutions) Electronic Co. for the particle size measurements.

Appendix A. Supplementary data

Supplementary data to this article can be found online at https://doi.org/10.1016/j.ceramint.2025.02.220.

References

[1] K. Beck, A.S. Ulrich, A.K. Czerny, E.M.H. White, M. Heilmaier, M.C. Galetz, Aluminide diffusion coatings for improving the pesting behavior of refractory metals, Surf. Coating. Technol. 476 (2024) 130205, https://doi.org/10.1016/j.surfcoat.2023.130205.

[2] B. Şenyurt, N. Akçamlı, D. Ağaoğulları, In-situ synthesis of tungsten boride-carbide composite powders from WO3-B2O3–Mg–C quaternary system via a mechanochemical route, Ceram. Int. 47 (2021) 1640–1650, https://doi.org/10.1016/j.ceramint.2020.08.280.

[3] C. Ren, R.K. Enneti, Latest developments in manufacturing and recycling of refractory materials, Jom 73 (2021) 3401–3402, https://doi.org/10.1007/s11837-021-04890-w.

[4] K.M. Mullin, C. Frey, J. Lamb, S.K. Wu, M.P. Echlin, T.M. Pollock, Materials & Design Rapid screening of single phase refractory alloys under laser melting conditions, Mater. Des. 238 (2024) 112726, https://doi.org/10.1016/j.matdes.2024.112726.

[5] S. Zhang, S.Y. Liu, D. Yan, Q. Yu, H. Ren, B. Yu, D. Li, Structural stability, hardness, fracture toughness and wear resistance of refractory metal carbonitrides RMC1-xNx (RM = Zr, Nb, Hf, Ta) solid solutions from first-principles calculations, Mater. Chem. Phys. 309 (2023) 128363, https://doi.org/10.1016/j.matchemphys.2023.128363.

[6] E. Zhao, J. Meng, Y. Ma, Z. Wu, Phase stability and mechanical properties of tungsten borides from first principles calculations, Phys. Chem. Chem. Phys. 12 (2010) 13158–13165, https://doi.org/10.1039/c004122j.

[7] J. Shinjo, C. Panwisawas, Chemical species mixing during direct energy deposition of bimetallic systems using titanium and dissimilar refractory metals for repair and biomedical applications, Addit. Manuf. 51 (2022) 102654, https://doi.org/10.1016/j.addma.2022.102654.

[8] Y. Wang, G.H. Zhang, X.B. He, B.J. Yan, Preparation of refractory metal diboride powder by reducing refractory metal oxide with calcium hexaboride, Ceram. Int. 45 (2019) 15772–15777, https://doi.org/10.1016/j.ceramint.2019.04.225.

[9] Q. Lin, Q. Huang, Y. Xu, Y. Cao, The mechanical, thermodynamic and electronic properties of TM2CrB2 borides with TM = V, Nb, Ta: a first-principles predictions, Solid State Commun. 368 (2023) 115184, https://doi.org/10.1016/j.ssc.2023.115184.

[10] W.G. Fahrenholtz, G.E. Hilmas, I.G. Talmy, J.A. Zaykoski, Refractory diborides of zirconium and hafnium, J. Am. Ceram. Soc. 90 (2007) 1347–1364, https://doi.org/10.1111/j.1551-2916.2007.01583.x.

[11] Y. Wang, Y.D. Wu, B. Peng, K.H. Wu, G.H. Zhang, A universal method for the synthesis of refractory metal diborides, Ceram. Int. 47 (2021) 14107–14114, https://doi.org/10.1016/j.ceramint.2021.01.281.

[12] İ. Süzer, S. Ates, A. Akbari, E. Aysel, S. Mertdinç-Ülküseven, C.F. Arisoy, M. L. Öveçoğlu, D. Ağaoğulları, Mechanochemical synthesis, purification, and optimization studies of Cr boride@MgO particles, Ceram. Int. 50 (2024) 11106–11118, https://doi.org/10.1016/j.ceramint.2024.01.012.

[13] Ö. Balci, D. Ağaoğullari, D. Ovali, M. Lütfi Öveçoğlu, I. Duman, In situ synthesis of NbB2-NbC composite powders by milling-assisted carbothermal reduction of oxide raw materials, Adv. Powder Technol. 26 (2015) 1200–1209, https://doi.org/10.1016/j.apt.2015.06.001.

[14] Ö. Balci, D. Ağaoğullari, I. Duman, M.L. Öveçoğlu, Carbothermal production of ZrB 2-ZrO 2 ceramic powders from ZrO 2-B 2O 3/B system by high-energy ball milling and annealing assisted process, Ceram. Int. 38 (2012) 2201–2207, https://doi.org/10.1016/j.ceramint.2011.10.067.

[15] Y.D. Wu, G.H. Zhang, Y. Wang, R. Xu, K.C. Chou, Synthesis of submicrometric VB2 powders by a boro-carbothermal reduction route, Ceram. Int. 45 (2019) 2492–2497, https://doi.org/10.1016/j.ceramint.2018.10.176.

[16] C. Ge, Q. Kou, J. Pang, J. Zhang, W. Jin, H. Zhu, G.M. Haarberg, S. Xiao, Preparation of ZrB2coatings by electrophoretic deposition in NaCl-KCl-AlCl3molten salts, J. Mater. Res. Technol. 20 (2022) 772–780, https://doi.org/10.1016/j.jmrt.2022.07.095.

[17] U. Fastner, T. Steck, A. Pascual, G. Fafilek, G.E. Nauer, Electrochemical deposition of TiB2 in high temperature molten salts, J. Alloys Compd. 452 (2008) 32–35, https://doi.org/10.1016/j.jallcom.2007.02.130.

[18] G. Kaptay, S.A. Kuznetsov, Electrochemical synthesis of refractory borides from molten salts, Plasma Ions 2 (1999) 45–56, https://doi.org/10.1016/s1288-3255(00)87686-8.

[19] R. Li, Y. Zhang, H. Lou, J. Li, Z. Feng, Synthesis of ZrB2 nanoparticles by sol-gel method, J. Sol. Gel Sci. Technol. 58 (2011) 580–585, https://doi.org/10.1007/s10971-011-2430-y.

[20] L. Bača, N. Stelzer, Adapting of sol-gel process for preparation of TiB2 powder from low-cost precursors, J. Eur. Ceram. Soc. 28 (2008) 907–911, https://doi.org/10.1016/j.jeurceramsoc.2007.09.028.

[21] A.K. Khanra, L.C. Pathak, M.M. Godkhindi, Double SHS of ZrB2 powder, J. Mater. Process. Technol. 202 (2008) 386–390, https://doi.org/10.1016/j.jmatprotec.2007.09.007.

[22] M. İpekçi, S. Acar, M. Elmadağlı, J. Hennicke, Ö. Balcı, M. Somer, Production of TiB2 by SHS and HCl leaching at different temperatures: characterization and investigation of sintering behavior by SPS, Ceram. Int. 43 (2017) 2039–2045, https://doi.org/10.1016/j.ceramint.2016.10.174.

[23] O. Balci, D. Ağaoğullari, C. Suryanarayana, I. Duman, M.L. Ovecoğlu, Synthesis and characterization of vanadium boride powders and their sintered bodies, Mater. Res. Express 6 (2019), https://doi.org/10.1088/2053-1591/ab2e56.

[24] Ö. Balcı, D. Ağaoğulları, M.L. Öveçoğlu, İ. Duman, Synthesis of niobium borides by powder metallurgy methods using Nb2O5, B2O3 and Mg blends, Trans. Nonferrous Metals Soc. China 26 (2016) 747–758, https://doi.org/10.1016/S1003-6326(16)64165-1.

[25] F.N. Çelik, E. Tekoğlu, S. Mertdinç, H. Gökçe, M.L. Öveçoğlu, D. Ağaoğulları, Mechanochemical synthesis investigations on the ternary and quaternary B2O3/TiO2/Mg/C systems, Solid State Sci. 128 (2022), https://doi.org/10.1016/j.solidstatesciences.2022.106897.

[26] R. Ricceri, P. Matteazzi, A fast and low-cost room temperature process for TiB2 formation by mechanosynthesis, Mater. Sci. Eng. A. 379 (2004) 341–346, https://doi.org/10.1016/j.msea.2004.02.064.

[27] C. Suryanarayana, Mechanical Alloying and Milling, 2001, p. 46.

[28] D. Ağaoğullari, Ö. Balci, M.L. Öveçoğlu, C. Suryanarayana, I. Duman, Synthesis of bulk nanocrystalline samarium hexaboride, J. Eur. Ceram. Soc. 35 (2015) 4121–4136, https://doi.org/10.1016/j.jeurceramsoc.2015.07.037.

[29] L. Takacs, Self-sustaining reactions induced by ball milling, Prog. Mater. Sci. 47 (2002) 355–414, https://doi.org/10.1016/S0079-6425(01)00002-0.

[30] V. Levitas, Continuum mechanical fundamentals of mechanochemistry. https://doi.org/10.1201/9781420034134.sec3, 2003.

[31] C. Suryanarayana, Mechanical alloying: a critical review, Mater. Res. Lett. 10 (2022) 619–647, https://doi.org/10.1080/21663831.2022.2075243.

[32] D. Ağaoğullari, I. Duman, M.L. Öveçoğlu, Synthesis of LaB 6 powders from La 2O 3, B 2O 3 and Mg blends via a mechanochemical route, Ceram. Int. 38 (2012) 6203–6214, https://doi.org/10.1016/j.ceramint.2012.04.073.

[33] D.V. Rybkovskiy, A.G. Kvashnin, Y.A. Kvashnina, A.R. Oganov, Structure, stability, and mechanical properties of boron-rich Mo-B phases: a computational study, J. Phys. Chem. Lett. 11 (2020) 2393–2401, https://doi.org/10.1021/acs.jpclett.0c00242.

[34] Y. Wang, H. Zhang, S. Jiao, K.C. Chou, G.H. Zhang, A facile pathway to prepare molybdenum boride powder from molybdenum and boron carbide, J. Am. Ceram. Soc. 103 (2020) 2399–2406, https://doi.org/10.1111/jace.16984.

[35] Y. Li, Y. Fan, Y. Chen, A novel route to nanosized molybdenum boride and carbide and/or metallic molybdenum by thermo-synthesis method from MoO3, KBH4, and CCl4, J. Solid State Chem. 170 (2003) 135–141, https://doi.org/10.1016/S0022-4596(02)00044-0.

[36] S.A. Kuznetsov, S.V. Kuznetsova, E.V. Rebrov, M.J.M. Mies, M.H.J.M. de Croon, J. C. Schouten, Synthesis of molybdenum borides and molybdenum silicides in molten salts and their oxidation behavior in an air-water mixture, Surf. Coating. Technol. 195 (2005) 182–188, https://doi.org/10.1016/j.surfcoat.2004.05.021.

[37] P.R. Jothi, Y. Zhang, J.P. Scheifers, H. Park, B.P.T. Fokwa, Molybdenum diboride nanoparticles as a highly efficient electrocatalyst for the hydrogen evolution reaction, Sustain. Energy Fuels 1 (2017) 1928–1934, https://doi.org/10.1039/C7SE00397H.

[38] J.K. Cochran, W.L. Daloz, P.E. Marshall, Oxidation resistant Mo-Mo 2B-silica and Mo-Mo 2B- silicate composites for high temperature applications, Jom 63 (2011) 44–49, https://doi.org/10.1007/s11837-011-0206-z.

[39] H. Park, A. Encinas, J.P. Scheifers, Y. Zhang, B.P.T. Fokwa, Boron-dependency of molybdenum boride electrocatalysts for the hydrogen evolution reaction, Angew. Chemie - Int. Ed. 56 (2017) 5575–5578, https://doi.org/10.1002/anie.201611756.

[40] K.E. Spear, P.K. Liao, The B-Mo (Boron-Molybdenum) system, Bull. Alloy Phase Diagrams 9 (1988) 457–466, https://doi.org/10.1007/BF02881867.

[41] H.E. Çamurlu, Preparation of single phase molybdenum boride, J. Alloys Compd. 509 (2011) 5431–5436, https://doi.org/10.1016/j.jallcom.2011.02.083.

[42] O. Torabi, R. Ebrahimi-Kahrizsangi, M.H. Golabgir, H. Tajizadegan, A. Jamshidi, Reaction chemistry in the Mg-B2O3-MoO3 system reactive mixtures, Int. J. Refract. Met. Hard Mater. 48 (2015) 102–107, https://doi.org/10.1016/j.ijrmhm.2014.07.040.
[43] S. Coşkun, M.L. Öveçoğlu, Room-temperature mechanochemical synthesis of W 2 B 5 powders, Metall. Mater. Trans. A Phys. Metall. Mater. Sci. 44 (2013) 1805–1813, https://doi.org/10.1007/s11661-012-1551-4.
[44] S.S. Setayandeh, J.H. Stansby, E.G. Obbard, M.I. Brand, D.M. Miskovic, K.J. Laws, V.K. Peterson, J.O. Astbury, C.L. Wilson, S. Irukuvarghula, P.A. Burr, A combined DFT and NPD approach to determine the structure and composition of the ε-phase of tungsten boride, Acta Mater. 259 (2023) 119282, https://doi.org/10.1016/j.actamat.2023.119282.
[45] J.M. Marshall, G. Singh, Proton and gamma irradiation of novel tungsten boride and carbide candidate shielding materials, Fusion Eng. Des. 193 (2023) 113667, https://doi.org/10.1016/j.fusengdes.2023.113667.
[46] M. Bahrami-Karkevandi, R. Ebrahimi-Kahrizsangi, B. Nasiri-Tabrizi, Formation and stability of tungsten boride nanocomposites in WO 3-B2O3-Mg ternary system: mechanochemical effects, Int. J. Refract. Met. Hard Mater. 46 (2014) 117–124, https://doi.org/10.1016/j.ijrmhm.2014.05.020.
[47] H. Itoh, T. Matsudaira, S. Naka, H. Hamamoto, M. Obayashi, Formation process of tungsten borides by solid state reaction between tungsten and amorphous boron, J. Mater. Sci. 22 (1987) 2811–2815, https://doi.org/10.1007/BF01086475.
[48] K. Ma, X. Cao, X. Xue, Mechanical properties, microstructure and grain orientation of hot pressed WB2 ceramics with Co as a sintering additive, Ceram. Int. 45 (2019) 14718–14727, https://doi.org/10.1016/j.ceramint.2019.04.196.
[49] S. Sugiyama, H. Taimatsu, Preparation of WC-WB-W2B composites from B4C-W-WC powders and their mechanical properties, Mater. Trans. 43 (2002) 1197–1201, https://doi.org/10.2320/matertrans.43.1197.
[50] T. Dash, B.B. Nayak, Preparation of multi-phase composite of tungsten carbide, tungsten boride and carbon by arc plasma melting: characterization of melt-cast product, Ceram. Int. 42 (2016) 445–459, https://doi.org/10.1016/j.ceramint.2015.08.129.
[51] J.V. Rau, A. Latini, R. Teghil, A. De Bonis, M. Fosca, R. Caminiti, V. Rossi Albertini, Superhard tungsten tetraboride films prepared by pulsed laser deposition method, ACS Appl. Mater. Interfaces 3 (2011) 3738–3743, https://doi.org/10.1021/am200927q.
[52] Y.C. Lin, Y.C. Lin, Elucidation of microstructure and wear behaviors of Ti-6Al-4V cladding using tungsten boride powder by the GTAW method, J. Coatings Technol. Res. 8 (2011) 247–253, https://doi.org/10.1007/s11998-010-9281-2.
[53] H. Park, Y. Zhang, E. Lee, P. Shankhari, B.P.T. Fokwa, High-current-density HER electrocatalysts: graphene-like boron layer and tungsten as key ingredients in metal diborides, ChemSusChem 12 (2019) 3726–3731, https://doi.org/10.1002/cssc.201901301.
[54] Y. Wang, Z.B. Li, K.F. Wang, G.H. Zhang, Preparation of Monophasic Tungsten boride powder from Tungsten and boron carbide, Ceram. Int. 47 (2021) 9543–9550, https://doi.org/10.1016/j.ceramint.2020.12.088.
[55] M. Usta, I. Ozbek, M. Ipek, C. Bindal, A.H. Ucisik, The characterization of borided pure tungsten, Surf. Coating. Technol. 194 (2005) 330–334, https://doi.org/10.1016/j.surfcoat.2004.06.042.
[56] H. Duschanek, P. Rogl, Critical assessment and thermodynamic calculation of the binary system boron-tungsten (B-W), J. Phase Equilibria 16 (1995) 150–161, https://doi.org/10.1007/BF02664852.
[57] S. Yazici, B. Derin, Effects of process parameters on tungsten boride production from WO 3 by self propagating high temperature synthesis, Mater, Sci. Eng. B. 178 (2013) 89–93, https://doi.org/10.1016/j.mseb.2012.10.008.
[58] P. Baláž, M. Achimovicová, M. Baláž, P. Billik, C.Z. Zara, J.M. Criado, F. Delogu, E. Dutková, E. Gaffet, F.J. Gotor, R. Kumar, I. Mitov, T. Rojac, M. Senna, A. Streletskii, W.C. Krystyna, Hallmarks of mechanochemistry: from nanoparticles to technology. https://doi.org/10.1039/c3cs35468g, 2013.
[59] S. Yazici, B. Derin, Production of tungsten boride from CaWO4 by self-propagating high-temperature synthesis followed by HCl leaching, Int. J. Refract. Met. Hard Mater. 29 (2011) 90–95, https://doi.org/10.1016/j.ijrmhm.2010.08.005.
[60] C.L. Yeh, W.S. Hsu, Preparation of molybdenum borides by combustion synthesis involving solid-phase displacement reactions, J. Alloys Compd. 457 (2008) 191–197, https://doi.org/10.1016/j.jallcom.2007.03.024.
[61] W.J. Choi, H. Lee, C.W. Park, Y. Do Kim, J. Byun, High temperature oxidation behavior of molybdenum borides by silicon pack cementation process, Int. J. Refract. Met. Hard Mater. 100 (2021) 105609, https://doi.org/10.1016/j.ijrmhm.2021.105609.
[62] K. Manukyan, S. Aydinyan, A. Aghajanyan, Y. Grigoryan, O. Niazyan, S. Kharatyan, Reaction pathway in the MoO 3 + Mg + C reactive mixtures, Int. J. Refract. Met. Hard Mater. 31 (2012) 28–32, https://doi.org/10.1016/j.ijrmhm.2011.09.001.
[63] S.V. Aydinyan, Z. Gumruyan, K.V. Manukyan, S.L. Kharatyan, Self-sustaining reduction of MoO3 by the Mg-C mixture, Mater. Sci. Eng. B. 172 (2010) 267–271, https://doi.org/10.1016/j.mseb.2010.05.028.
[64] O. Torabi, M.H. Golabgir, H. Tajizadegan, H. Torabi, A study on mechanochemical behavior of MoO3-Mg-C to synthesize molybdenum carbide, Int. J. Refract. Met. Hard Mater. 47 (2014) 18–24, https://doi.org/10.1016/j.ijrmhm.2014.06.001.
[65] Z. Wu, Y. Long, H.T. Lin, F. Zhang, Effect of tantalum on phase transition and thermal stability of metastable tungsten tetra-boride, Ceram. Int. 46 (2020) 17217–17223, https://doi.org/10.1016/j.ceramint.2020.03.294.
[66] M. Jalaly, M.S. Bafghi, M. Tamizifar, F.J. Gotor, Mechanosynthesis of nanocrystalline ZrB2-based powders by mechanically induced self-sustaining reaction method, Adv. Appl. Ceram. 112 (2013) 383–388, https://doi.org/10.1179/1743676113Y.0000000091.
[67] N.Ö. Aytekin, D. Ağaoğullari, M.L. Öveçoğlu, Mechanochemical synthesis of tungsten carbide powders induced by magnesiothermic reduction of WCl6 and Na2CO3 raw materials, Mater. Res. Express 6 (2019), https://doi.org/10.1088/2053-1591/ab2c34.
[68] S. Coşkun, M.L. Öveçoğlu, Room-temperature mechanochemical synthesis of W 2 B 5 powders, Metall. Mater. Trans. A Phys. Metall. Mater. Sci. 44 (2013) 1805–1813, https://doi.org/10.1007/s11661-012-1551-4.
[69] J. Ghorbantabar Omran, M. Sharifitabar, M. Shafiee Afarani, On the self-propagating high-temperature synthesis of tungsten boride containing composite powders from WO3–B2O3–Mg system, Ceram. Int. 44 (2018) 14355–14362, https://doi.org/10.1016/j.ceramint.2018.05.044.
[70] A.Y. Potanin, Y.S. Pogozhev, E.A. Levashov, A.V. Novikov, N.V. Shvindina, T. A. Sviridova, Kinetics and oxidation mechanism of MoSi2–MoB ceramics in the 600–1200 °C temperature range, Ceram. Int. 43 (2017) 10478–10486, https://doi.org/10.1016/j.ceramint.2017.05.093.
[71] E. Soylu, F. Kaya, M. Sezen, F. Bakan, G. Tranell, B. Derin, On the production of W–Fe–B ternary compounds by self-propagating high-temperature synthesis, Metall. Mater. Trans. B Process Metall. Mater. Process. Sci. 53 (2022) 3624–3634, https://doi.org/10.1007/s11663-022-02625-z.
[72] Y. Lin, C. McFadzean, S.A. Humphry-Baker, Oxidation resistance of WB and W2B-W neutron shields, J. Nucl. Mater. 565 (2022) 153762, https://doi.org/10.1016/j.jnucmat.2022.153762.
[73] C.L. Yeh, H.J. Wang, Preparation of tungsten borides by combustion synthesis involving borothermic reduction of WO3, Ceram. Int. 37 (2011) 2597–2601, https://doi.org/10.1016/j.ceramint.2011.04.006.
[74] S. Okada, T. Atoda, I. Higashi, Y. Takahashi, Preparation of single crystals of MoB2 by the aluminium-flux technique and some of their properties, J. Mater. Sci. 22 (1987) 2993–2999, https://doi.org/10.1007/BF01086503.